Beam Tests of Ionization Chambers for the NuMI Neutrino Beam

Robert M. Zwaska, James Hall, Sacha E. Kopp, Marek Proga, Albert Erwin, Christos Velissaris, Debbie Harris, Donna Naples, Jeff McDonald, David Northacker, Milind Diwan, and Brett Viren

***Abstract*— We have conducted tests at the Fermilab Booster of ionization chambers to be used as monitors of the NuMI neutrino beamline. The chambers were exposed to proton fluxes of up to 10^{12} particles/cm^2/1.56μs. We studied potential space charge effects which could reduce signal collection from the chambers at large charged particle beam intensities.**

***Index Terms*— Ionization chambers, ionizing radiation, multiplication, neutrinos, particle beam measurements, space charge.**

I. Introduction

VALIDATION of the NuMI (Neutrinos at the Main Injector) neutrino beam requires continuous monitoring of the conjugate hadron and muon beams. The NuMI beam is composed primarily of muon neutrinos from the decays of pions. The pions are produced by the interactions of 120 GeV protons from the Fermilab Main Injector which impinge on a graphite production target. Focusing magnets, called horns, steer positive pions into an evacuated tunnel where they decay to muons and neutrinos. A downstream Aluminum/Steel absorber and bedrock absorb the remnant hadrons and muons in the beam, leaving only neutrinos. The facility is expected deliver beam to neutrino experiments, beginning with the MINOS neutrino oscillation experiment, starting in early 2005.

The beam monitoring system will measure the intensity and spatial distribution of the hadron beam at the end of the decay tunnel, upstream of the absorber, and of the muon beam after the absorber and at several stations in the bedrock. The monitoring system will consist of 2 m $\times$ 2 m arrays of ionization chambers with 25 cm inter-chamber spacing, with one chamber array in each of the above stations. The hadron and muon ßuxes are measures of any missteering or focusing failures. The peak charged particle ßuxes in one 9 μs accelerator burst will be 2000, 25, 3, and 1.5×10^6/cm^2 in the four monitoring stations.

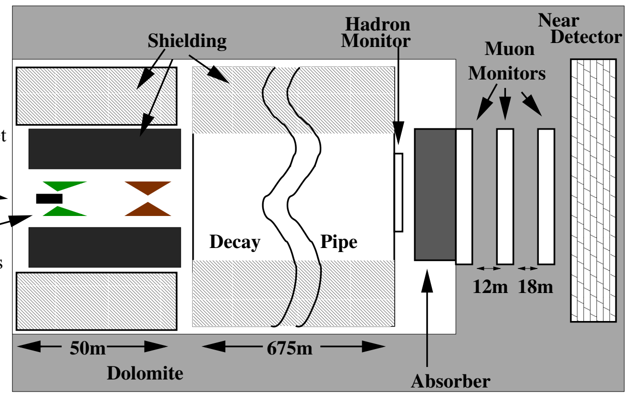

Fig. 1. Pictorial diagram of the NuMI beamline. The 120 GeV proton beam is incident on the target producing a hadron beam. The positive hadrons are focused by the horns, of which the pions travel into the decay pipe where they decay into muons and muon neutrinos, making the neutrino beam. The hadron monitor and muon monitors measure hadron and muon ßuxes at their locations and are constructed of the ion chambers described herein.

Each ionization chamber will measure the ßux of charged particles by using an applied electric Þeld to collect the ionization created in a helium gas volume. The charge measured from each chamber will be proportional to the charged particle ßux at that location. By using an array of chambers the spatial distribution of beam intensity can be inferred. While operated without gas ampliÞcation the signal from the intense NuMI beam in one 8 cm $\times$ 8 cm ionization chamber will be 33000, 1400, 170, and 83 pC at the four stations.

The major limitation of ionization chambers used as beam monitors has been space charge build up inside the chamber. Intense particle ßuxes release sufÞcient ionized charge in the chamber gas so as to create a reverse electric Þeld which reduces the electric Þeld inside the chamber. With the reduced net Þeld in the chamber, ions require longer time to reach the collection electrodes, and hence suffer more recombination loss in the gas. Recombination losses increase at larger particle ßuxes, resulting in a non-linear performance of the ionization chamber beam monitor at large intensities.

The NuMI Beam Monitoring parallel plate ionization chambers are made up of two 4Ó square ceramic plates with Ag-Pt electrodes. One plate has a single electrode that applies HV bias. The second plate has two electrodes: a central square sense

Manuscript received November 12, 2002; This work was supported by the U.S. Department of Energy, DE-AC02-76CH3000 and DE-FG03-93ER40757, DE-FG02-05ER40896, and the Fondren Foundation.

R. M. Zwaska, J. Hall, S. E. Kopp, and M. Proga are with the Department of Physics, University of Texas at Austin, Austin, TX 78712 USA (e-mail: zwaska@mail.hep.utexas.edu; kopp@mail.hep.utexas.edu).

A. Erwin and C. Velissaris are with the Department of Physics, University of Wisconsin at Madison, Madison, WI 53706 USA.

D. Harris is with the Fermi National Accelerator Laboratory, Batavia, IL 60510 USA.

D. Naples, J. McDonald, and D. Northacker are with the Department of Physics, University of Pittsburgh, Pittsburgh, PA 15260 USA.

M. Diwan and B. Viren are with the Brookhaven National Laboratory, Upton, NY 11973 USA.

pad measuring 3Ó× 3Ó,surrounded by a 1 cm guard ring. The sense pad is connected into the electronics which sees a virtual ground. The guard ring is grounded. The chamber gas is pure helium at atmospheric pressure.

II. Booster Beam Test

A beam test of prototype ionizations chambers was undertaken at the Fermilab Booster accelerator, which delivers up to 10^{12} protons/cm^2 of 8 GeV in a 1.56 μsec spill. Tested were two chambers, one with a 1 mm electrode spacing, the other with 2 mm, under Helium gas ßow. We studied the shape of the ionization vs. voltage plateau curve at several intensities and the linearity of the chamber response vs. beam intensity at several applied voltages.

For our beam test we placed two ionization chambers in the beamline. The chambers were housed in a stainless steel vessel with .005ÓTi beam entrance and exit windows. Electrical feedthroughs were made with stainless steel compression Þttings and PEEK plastic.

Helium was supplied from a cylinder with 99.998% purity. It was Þrst passed through a getter and gas analyzer. Online measurement indicated impurites of $<$ 1.5 p.p.m. All gas seals were metallic consisting of compression Þttings or copper gaskets compressed by vacuum Þttings.

Upstream of our ion chamber vessel Fermilab provided a secondary emission monitor (SEM), to locate the beam. The SEM provided targeting information upstream of the chamber, but was not usable in the analysis because the beam diverged after passing through the SEM, and it was only capable of measuring either the horizontal or vertical proÞle at any given time. Furthermore, the SEM was insensitive below 2×10^{11} protons per pulse. During the portion of datataking above 2×10^{11} the SEM indicated constant spot size.

A beam toroid was the primary method of measuring the beam intensity delivered to the apparatus. The toroid was supplied with an ampliÞer and ADC whose least signiÞcant bit was 5×10^9 protons.

Rigidly attached on the outside of the ion chamber vessel were two beam proÞle chambers fashioned out of G-10 circuit board and epoxy. Each chamber had a segmented signal electrode composed of $1{\times}10$ cm^2 strips. One chamber provided the vertical proÞle, the other the horizontal proÞle. The proÞle chambers were the primary method for determining beam size. Gas ßow was the same as that passed through the vessel. The proÞle chambers indicated constant beam spot size $\sim$5 cm^2.

The signal from each of the ion chambers and beam proÞle chambers were read out into a charge integrating ampliÞer and then into an ADC [1]. The electronics were triggered on an accelerator clock signal shortly before the beam pulse. The charge integration time could be altered and taken between beam spills, allowing measurement of pedestals and backgrounds.

III. Experimental Results

Tests of the chambers consisted of two complementary measurements. The Þrst held the beam intensity constant, while

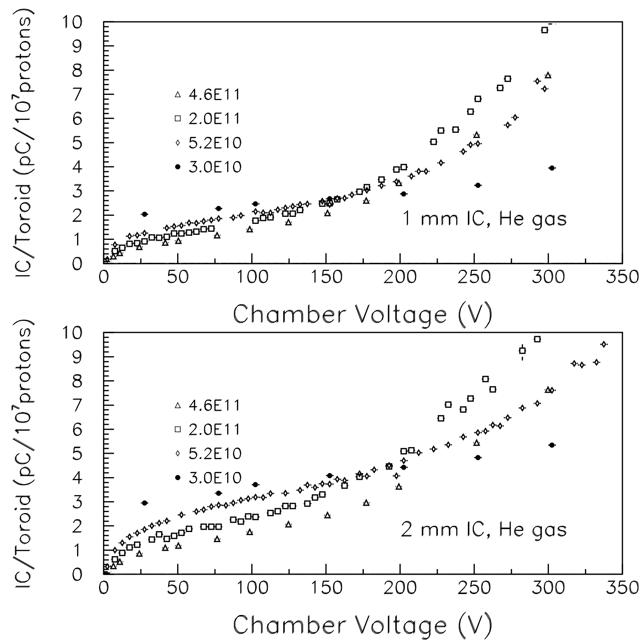

Fig. 2. High voltage scans of the 1 and 2 mm ion chambers (ICÕs) in Helium at various beam intensities. The vertical axis is the ratio of charge collected to the beam intensity measured by the toroid.

varying the voltages applied to the chambers. The second held the applied voltages constant while adjusting the beam intensity.

The results of the Þrst test are displayed in Fig. 2. Each chamber is subjected to four beam intensities and the voltage varied 0-350 V. The ratio of collected charge to the measured beam intensity is plotted as a function of applied voltage.

The ideal voltage plateau curve would consist of a quick rise to a constant charge collected per proton, independent of voltage and intensity. This constant charge collected would be equal to the amount of charge liberated in the gas per proton. At higher voltages gas ampliÞcation is expected and charge collected per proton would increase above the plateau. From the height of the plateau on the 1 mm chamber one may infer a charge ionized per proton of 2.6 pC/10^7 protons, or 1.6 electron-ion pairs per proton incident on a 1 mm gas gap. This value of 16 ionizations / cm is in agreement with some published values for pure Helium [2].

The drifting ions and electrons inside the chamber establish their own electric Þeld. This space charge induced electric Þeld screens the electrodes, slowing the transit of ions and electrons across the electrode gap. As discussed extensively in [3]-[7], operating ion chambers at very large particle ßuences modiÞes the voltage plateau curve discussed above. If the speed of the charges is sufÞciently slowed, recombination may take place. This situation is especially evident $<$150 V, where the lower voltages result in slower ion drift velocities and longer ion transit times. This loss also increases where space charge buildup would be worse, *e.g.* at higher beam intensity or in a larger gap chamber.

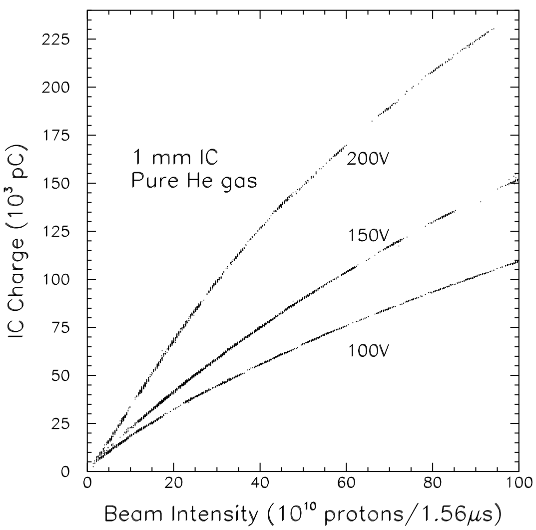

Fig. 3. Beam intensity scans of the 1 mm ion chamber in Helium at various voltages.

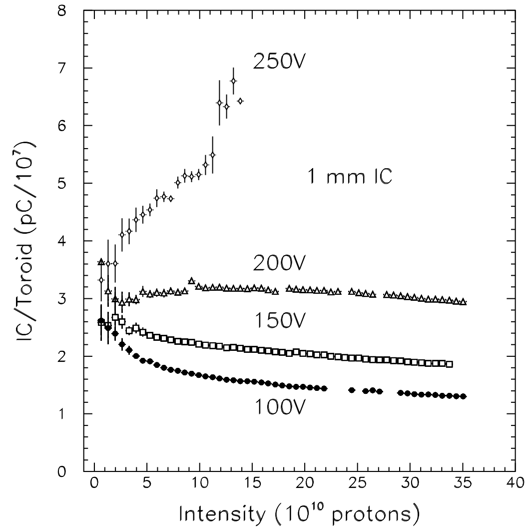

Fig. 4. Normalized beam intensity scans of the 1mm ion chamber at various voltages. Here, the vertical axis is the ratio of charge collected to the beam intensity as measured by the toroid.

Space charge effects were evident at all of the intensities delivered by the Booster. In Fig. 2 all of the curves, except possibly one, show a slope in the plateau region, suggesting that there is little or no region where the charge is collected without loss or gain. The only useful voltage looks to be 130-190 V for the 1 mm chamber, where the curves all intersect. In Section IV we analyze this in terms of competing recombination and multiplication effects in the gas.

Fig. 3 displays the results of the second test performed in our beam test for the case of the 1 mm chamber. The collected charge on the ion chamber is plotted as a function of beam intensity for several applied voltages. Here, ideal curves would all join at low intensity. Recombination loss, especially visible for lower voltages, cause the curves to fall off at higher intensity. The linear region is the operating range for the chamber where charge collected is proportional to incident ßux.

An analysis of the 200 V curve up to 20×10^{10} gives a good linear Þt (χ^2/N_{DOF} = 456/625). However, the intercept is less than zero: (-0.05 $\pm$ 0.012) $\times 10^3$ pC.

The nonzero intercept is more apparent when the curve is plotted residually, as in Fig. 4 where the ratio of charge collected to beam intensity is plotted versus intensity. Here a straight line with zero intercept in the previous plot would be a horizontal line. Here the 200 V curve is relatively ßat when the intensity is $< 2 \times 10^{11}$ protons, but it is obviously curved upward then downward. In Section IV we discuss how the interplay of multiplication and recombination can cause such an effect. Similar to the voltage plateau data, the data in Figure 4 indicate $\sim$3pC/10^7 protons, or 18 electron-ion pairs per cm in the He.

IV. Simulation

In this section we interpret the data collected at the Booster beam test using a computer simulation of the pulse development in an ion chamber. The simulation incorporates the known drift of electrons and of Helium ions in electric Þelds, the effects of volume recombination of charges, and of gas ampliÞcation. The simulation follows the charges during and after the beam spill, recording the net charge collected at the chamber electrodes. The simulations indicate a complex interplay between gas ampliÞcation and charge recombination as a result of space charge build up. This calculation will then be used to extrapolate to the particle ßuxes and 8.6μsec spill duration expected in NuMI.

A. Simulation Method

The differential equations governing the charge ßux and electric Þeld evolution inside the ion chamber are nonlinear. Some earlier work analyzed special cases. Boag [6] demonstrated that space charge accumulation in a continuously-ionized chamber causes the formation of a Òdead regionÓof no electric Þeld, and makes the approximation that all charges in the dead region are lost due to recombination. In Ref [7], an ion chamber ionized over a short duration is studied, but again the assumption is made that all charges in the dead zone are lost to recombination. That assumption is not valid for our experiment where the beam pulse is of short duration allowing the dead zone to disappear before the charge completely recombines.

The present work considers the time dependant case where ionization is deliverd in short pulse of 1.6 μs and allowed to drift out of the chamber. Our simulation is a Þnite element calculation of one spatial dimension, such that there are series of inÞnite planes of charge between the electrodes. The electrons and ions are drifted with the velocites discussed in Section

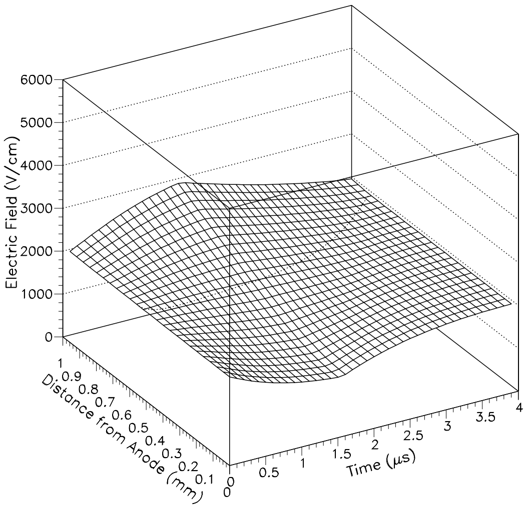

Fig. 5. Simulated electric Þeld evolution in terms of position and time for a 1 mm ion chamber operated at 200 V with ionization of 10^{10} ion./cc/μs for 1.6 μs. Small electric Þeld disruptions due to space charge accumulation occur as the beam pulse develops.

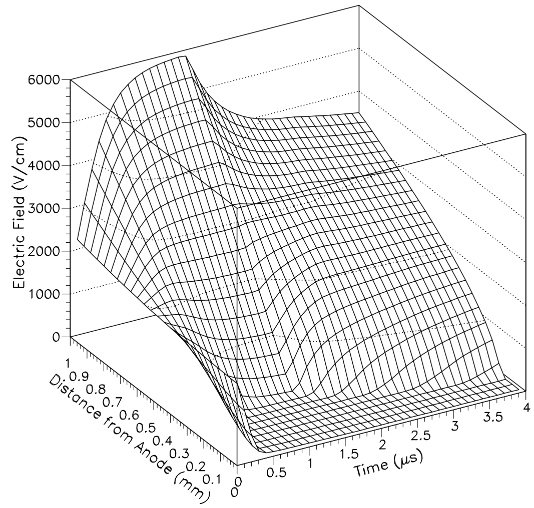

Fig. 6. Simulated electric Þeld evolution in terms of position and time for a 1 mm ion chamber operated at 200 V with ionization of 10^{11} ion./cc/μs for 1.6 μs. A Òdead zoneÓ region with a very low electric Þeld forms at about 0.3 μs into the beam spill, and eventually grows to cover a third of the chamber. The space charge accumulation also increase the electric Þeld in part of the chamber to the point where the maximum electric Þeld at the cathode is almost three times the applied electric Þeld.

IV-B. Space charge is calculated at each step and an image charge is induced such that the potential difference betweeen the electrodes is maintained at the applied voltage.

Simulated electric Þeld distributions are shown in Figs. 5 and 6. The Þgures show the Þeld development using only the charge transport, and ignore charge recombination or multiplication. Fig. 5 is at a modest intensity where the excess of ions slightly warps the Þeld. In Fig. 6, the ion excess is much greater, to the point where it entirely screens the anode from the applied Þeld, creating a dead zone. As ionization continues in the dead zone the ion and electron densities there increase because the charges are effectively trapped. When the beam spill ends the dead zone slowly fades away. Charge is able to escape from the edge of the dead zone because the dead zone is not created by the charge inside, but the excess of ions outside of it.

B. Gas Properties

The parameters of charge drift, loss, and ampliÞcation have been taken from several literature sources. The electron drift velocities as a function of electric Þeld are taken from Ref [8]. For the drift of Helium, we use the mobility for the He_2^+ ion, $\mu_{He_2^+} = 20\,\mathrm{cm}^2/(\mathrm{V}\cdot\mathrm{s})$ [8], following the discussion of [9] which notes that above pressures of a few Torr, He^+ ions tend to collide in the gas and form molecular ions. Previous work [10], [11] have cited 10 cm^2/(V·s), the mobility for He^+.

Volume recombination of electrons and ions through two- and three-body processes at atmospheric pressure are the dominant method of charge loss. RefÕs [8] and [12] parameterize recombination of the form: $dn_-/dt = dn_+/dt = -rn_-n_+$, with n_+ (n_-) the positive (negative) ion densities in the gas, and the measured recombination coefÞcient $r = 2.4 \times 10^{-8}$ cm^3/(ion·s). Using the data from Ref [11] and [12] we Þnd that the attachment of electrons to electronegative impurities in the gas is insigniÞcant for impurity levels less than 30p.p.m. (c.f. 1.5p.p.m. for our chambers), so is not simulated.

Charge ampliÞcation in the chamber gas is modeled via $dN/dx = N\alpha$, with the Townsend coefÞcient α modelled via $\alpha/P = A\exp[-B/(X/P)]$, where P is the chamber gas pressure, X is the applied electric Þeld, and the parameters $A = 3$ ion pairs/(cm-Torr) and $B = 25$ V/(cm-Torr) [13]. This parameterization is taken from a source with similar gas purity, which is of importance because the purest Helium gas has signiÞcantly lower Townsend coefÞcient but is sensitive to even a few p.p.b. impurity level [8].

The ionization rate in the simulation is quoted in units of ionizations/cm^2/μs in order to factor out the question of how many ionizations are created by an incident proton. Given dE/dx and W values for Helium, values of 8-16/cm have been derived [2], [10], [11], [14], but this too is sensitive to impurity level. For comparison to our data in the 1 mm chamber, 1 ion./cc/μs $\approx$ 0.6 protons/spill if the beam spot size of 5 cm^2 and $\sim$16 ionizations/cm in Helium [2] are used.

C. Simulation Results

We found that the simulated space charge accumulation causes not only recombination losses, but the high Þelds also cause signiÞcant multiplication. This result can be seen in Fig. 7 where the charge collected per ionization can actually increase with ionization, until recombination takes over. This should be compared to Fig. 4. Both the data and the simulation indicate

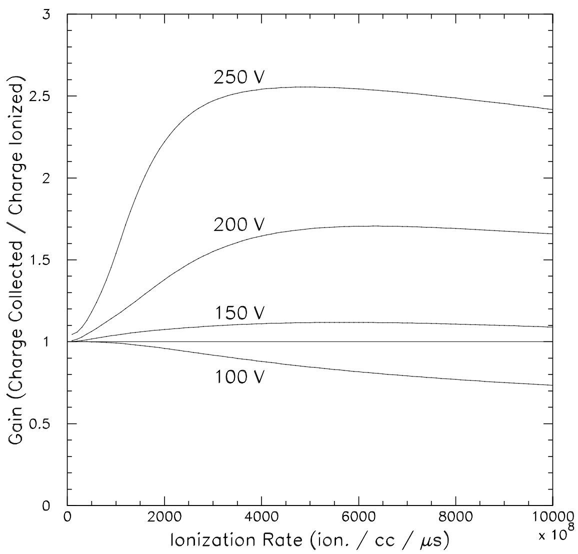

Fig. 7. Simulated normalized intensity scans of a 1 mm in chamber operated at various voltages where charge recombination and gas multiplication are included. The vertical axis is the ratio of charge collected to the amount of charge initially ionized in the chamber (i.e. excluding the effects of recombination and multiplication).

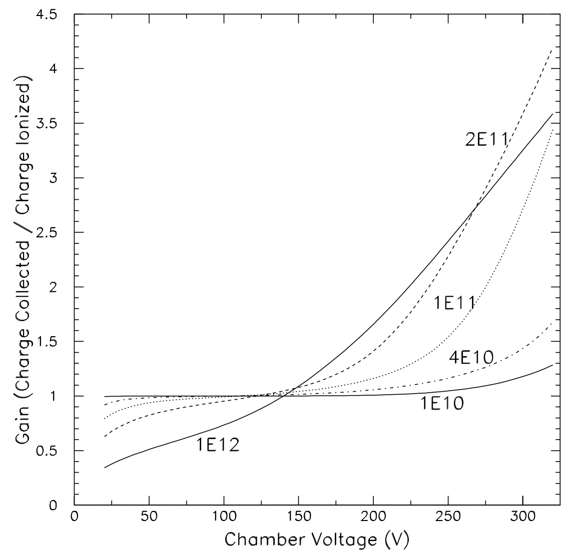

Fig. 8. Simulated voltage scans of a 1 mm ion chamber operated at various intensities where charge recombination and gas multiplication are included. The vertial axis is the ratio of charge collected to the amount of charge initially ionized in the chamber (i.e. excluding the effects of recombination and multiplication).

such an effect. This feature of the curve makes the Þt line have a negative intercept, as referenced earlier. The lower voltage required in the simulation to generate this effect suggests that multiplication may be overstated in simulation.

Fig. 8 can also be compared to Fig.2. The behavior is rather complicated, but is marked by greater losses at high intensity and low voltage, and also by a crossing point where the curves all approach each other. In the simulation this occurs at $\approx$140V, and that the higher intensities show gain at lower voltages. This behavior is nominally reproduced in the data. The crossing point which occurs at a lower voltage in the simulation, again suggesting that multiplication is overstated there. The crossing point can be moved left and right by simply changing the value of α, and is particularly sensitive to the parameter B. Hence the data can constrain the value of α, and possibly r for recombination.

V. Conclusion

We have performed a beam test of Helium-Þlled ionization chambers at the Fermilab Booster accelerator. We have compared our experimental results to our own calculation of the expected charge collection in such chambers. While we have yet to extrapolate our calculations to the anticipated NuMI beam environment using the constraints of our beam test data, several effects of interest are observed. Similar to previous work, our results indicate that space charge effects induce recombination losses in the collected charge at high particle ßuxes, and our data is in quantitative agreement with the loss predicted by volume recombination. However, our calculations indicate additionally that gas ampliÞcation occurs in the ion chambers at high beam intensities due to the large space charge build-up of the electric Þeld. The gas ampliÞcation gains compete with the losses due to recombination, effectively extending the range of linear response of the ion chamber with respect to beam intensity.

References

[1] W. Kissel, B. Lublinsky and A. Frank, ÒNew SWIC Scanner/Controller System,Ó presented at the 1995 International Conference on Accelerator and Large Experimental Physics Control Systems, 1996.

[2] K. Hagiwara *et al.*, ÒReview of Particle Properties,Ó *Phys. Rev. D*, vol. 66, 010001, 2002.

[3] D. H. Wilkinson, *Ionization Chambers and Counters*, Cambridge University Press, Cambridge, 1950.

[4] B.Rossi and H.Staub, Ionization Counters and Detectors, McGraw-Hill, New York, 1949.

[5] G. F. Knoll, *Radiation Detection and Measurement*, Third Edition, John Wiley & Sons, Inc., New York, 2000.

[6] J. W. Boag and T. Wilson, ÒThe saturation curve at high ionization intensity,Ó *Brit. J. Appl. Phys.,* vol. 3, pp. 222-229, 1952.

[7] S. Palestini, G. D. Barr, C. Biino, P. O. CalaÞura, A. Ceccucci, C. Cerri *et al.*, ÒSpace Charge in ionization detectors and the NA48 electromagnetic calorimeter,Ó *Nucl. Inst. Meth. A*, vol. 421, pp. 75-89, 1999.

[8] J. Dutton, ÒA Survey of Electron Swarm Data,Ó *J. Phys. Chem. Ref. Data*, vol. 4, pp. 577-856, 1975.

[9] L. B. Loeb, *Basic Processes of Gaseous Electronics*, University of California Press, Berkeley, California 1955.

[10] W. Blum, L. Rolandi, *Particle Detection with Drift Chambers*, Berlin, Springer-Verlag, 1994.

[11] F. Sauli, ÒPrinciples of Operation of Multiwire Proportional and Drift Chambers,Ó CERN preprint CERN-77-09 (3 May 1977).

[12] S. Brown, *Basic Data of Plasma Physics: The Fundamental Data on Electrical Discharges in Gases*, AIP Press, New York, 1994.

[13] A. von Engel, *Ionized Gases*, Springer-Verlag, New York, 1995.

[14] ICRU, International Commission on Radiation Units and Measurements, *Average Energy Required to Produce an Ion Pair*, ICRU Report 31, ICRU, Wahington D. C., 1979.